J Nanopart Res (2011) 13:1841–1853
DOI 10.1007/s11051-010-9932-3

RESEARCH PAPER

Enhanced mechanical strength of hydroxyapatite nanorods reinforced with polyethylene

A. Joseph Nathanael · D. Mangalaraj · P. Chi Chen · N. Ponpandian

Received: 3 June 2009 / Accepted: 12 April 2010 / Published online: 27 April 2010

Abstract Hydroxyapatite (HAp) nanostructures may be an advanced candidate in biomedical applications for an apatite substitute of bone and teeth than other form of HAp. In contrast, well-defined size and shape control in synthesizing HAp nanostructures is always difficult. In this study, hydroxyapatite nanorods (HAp NRs) were prepared by simple hydrothermal method with controlling the reaction time without using any surfactant or templating agents. The nanostructure clearly depicts the growth stages of the HAp NRs by increasing the reaction time. The synthesized HAp has the rod like morphology with uniform size distribution with the aspect ratio of about 8–10. Transmission electron microscopic (TEM) and high resolution TEM (HRTEM) images show that the growth direction of the HAp is parallel to the (001) plane. The interplanar distances measured in segments (fringes) of the HRTEM micrograph were ~0.35 nm, corresponding to the interplanar spacing of the (002) plane of the hexagonal HAp. X-ray diffraction (XRD) measurements indicate that the improved crystallinity of the HAp by increasing the reaction time. The mechanical studies reveal that the improved tensile strength and the abrasion resistance are observed for the HAp nanorods reinforcing with high molecular weight polyethylene (HMWPE).

Keywords Nanorods · Hydroxyapatite · Polyethylene · TEM · Mechanical properties · Biocompatible implants · Nanomedicine

A. Joseph Nathanael
Thin Film and Nanomaterials Laboratory, Department of Physics, Bharathiar University, Coimbatore 641 046, India

D. Mangalaraj (✉) · N. Ponpandian
Department of Nanoscience and Technology, Bharathiar University, Coimbatore 641 046, India
e-mail: dmraj800@yahoo.com

P. Chi Chen
Department of Chemical and Materials Engineering, Lunghwa University of Science and Technology, Taoyuan, Taiwan ROC

Introduction

Hydroxyapatite (HAp, $Ca_{10}(PO_4)_6(OH)_2$) has been extensively used in medicine as implantable materials, owing to its good biocompatibility, bioactivity, high osteoconductive, and/or osteoinductive properties (Elliott 1994; Hench 1991). Synthesis of one dimensional (1-D) HAp powders has been attracting attention in recent years because of the great potential applications of 1-D nanostructures, such as nanotubes, nanofibers/nanowires, and nanorods. The size and morphology would largely determine the properties of certain material. Bone itself is a composite consisting of HAp nanorods embedded in the collagen matrix. Hence, HAp nanorods are desirable when biocompatibility is concerned (Zhang et al. 2005). HAp is also the main component of the mineral part

of bone tissue, tooth enamel, and dentin. Synthetic HAp is biocompatible with the human body and is widely used in medicine as a material for bone tissue regeneration (Hulber et al. 1987; Rodriguez-Lorenzo and Vallet-Regi 2000). It is also a promising material for reinforcing filler for composites (Lin et al. 2007). It is not only a main component of hard tissues, such as bones and teeth, but also a material applied for bioceramics, adsorbents, and catalysts (Di et al. 2004; Zhu et al. 2004; Anmin et al. 2006). In recent years, with the growing necessity of biomaterials, HAp has drawn extensive attention. However, the HAp bioceramics cannot be used for heavy load-bearing applications, like artificial teeth or bones because of their poor mechanical properties. Thus, regardless of their favorable biological properties, the poor mechanical properties of HAp bioceramics have severely hindered their clinical applications (Hench 1991; Yaszemski et al. 1996). Therefore, a number of studies have been focused on the improvement of the mechanical properties of HAp bioceramics (Shen et al. 2001; Suchanek et al. 1997), and studies have shown that the mechanical properties of the ceramics could be reinforced remarkably by one dimensional (1-D) nanoscale building blocks such as nanorods, nanofibers, and nanotubes (Ramay and Zhang 2004; Yang et al. 2004; Kobayashi and Kawai 2007).

However, ultrastructural examination of deproteinated bone reveals that individual 25–50 nm HAp crystal is the essence of bone in terms of mechanical properties and bioresorbability, and plays an important role in biomineral formation (Shi et al. 2009). This nano-HAp has special characteristics such as improved biocompatibility, good bioactivity, and flexible structure (Huang et al. 2007; Lewandrowski et al. 2003), which are important for their potential applications in medicine. However, it is always difficult to synthesize nano-HAp particles with well-defined sizes (Feng et al. 2005). Therefore, many research works have been focused on the synthesis of 1-D HAp nanostructures.

Polymer/ceramic composites scaffolds mimic the natural bone to some extent. Scaffolds were initially composed of either polymer or ceramic, which, however, tended to be too flexible or too brittle, respectively (Maquet et al. 2004). In the past few years, polymer/ceramic composites have therefore gained increased interest in the field of tissue engineering to reconstruct several types of structural tissues, such as bone, cartilage, tendons or ligaments, and tissue interfaces (Wang 2003). The composite is expected to have improved mechanical properties compared to the pure polymer, and better structural integrity and flexibility than brittle ceramics. In fact, the combination of ceramic and polymer could provide reinforced porous structures with enhanced bioactivity, mechanical strength and controlled resorption rates. Also the composite materials have been considered better choices as bone tissue engineering scaffolds (Mathieu et al. 2006).

Earlier work on HAp was mainly emphasized upon controlling the stoichiometry of the products, whereas with the development of nanotechnologies, considerable effort is now focused on controlling the morphology and size (Walsh and Mann 1996; Sarda et al. 1999; Hirai et al. 2000; Yuan et al. 2002) because studies have shown that many clinical capabilities of HAp mainly depend on their morphology and size (Elliott 1998). Natural bone is composed of inorganic and organic compounds. The nanometer size of the inorganic component (mainly bone like apatite) in natural bone is considered to be important for the mechanical properties of the bone. In addition, nano-sized HAp may have other special properties due to its small size and huge specific surface area (Wei and Ma 2004). Therefore, synthesis of nanoscale HAp will largely improve their clinical applications. Among the reported studies, however, a few works dealt with the preparation of HAp [$Ca_{10}(PO_4)_6(OH)_2$] nano structures. Most of the HAp nanostructures were prepared by using surfactants or templating agents (Zhang et al. 2005; Lin et al. 2007; Wang et al. 2006a; Shiha et al. 2005; Sun et al. 2007; Wang et al. 2006b; Sun et al. 2006; Chen et al. 2007; Cao et al. 2004). As mentioned earlier, bone is a composite consisting of HAp nanorods.

Hence this study is mainly focused on the size scale and structure of HAp, and aim at elucidating the enhanced mechanical property of HAp NRs. Herein, we report the synthesis of HAp NRs using only Ca and P sources in hydrothermal method by changing the reaction time without any addition of surfactant and/or templating agents to study the effect of morphological variations and their influence on the mechanical properties. The mechanical properties of the HAp nanorods reinforced with high molecular weight polyethylene (HMWPE) was done by reinforce 10 wt% HAp nanorods with HMWPE and for comparison, the measurements on pure HMWPE and

10 wt% precipitated HAp reinforced with HMWPE were also carried out.

Materials and methods

Synthesis

In a typical synthesis process, calcium nitrate ($Ca(NO_3)_2{\cdot}4H_2O$) and diammonium hydrogen phosphate ($(NH_4)_2HPO_4$) were used as calcium and phosphate sources, respectively. The HAp was prepared by taking calcium nitrate and diammonium hydrogen phosphate separately and mixed with deionized water with the molar ratio of 1:0.6 in order to maintain the Ca/P ratio 1.67 which is the stoichiometric molar ratio of HAp. The pH of the phosphate containing solution was increased to 9 by adding ammonium hydroxide (30%). During the reaction, the P containing solution was added dropwise into the Ca containing solution with vigorous stirring for 1 h. The mixed solution was transferred to the Teflon beaker of the stainless steal autoclave and placed in the oven at 180 °C for 6, 12, 18, and 24 h, respectively, for reaction. After the reaction, the autoclave was cooled down to room temperature automatically. The final precipitates were washed several times with distilled water and dried at 100 °C overnight. The dried powders were crushed with mortar and pestle and calcined at 600 °C for 2 h.

The equation of the chemical reaction is:

$$10Ca(NO_3)_2{\cdot}4H_2O + 6(NH_4)_2HPO_4 + 8NH_4OH \rightarrow Ca_{10}(PO_4)_6(OH)_2 + 20NH_4NO_3 + 46H_2O$$

For mechanical strength analysis, a HMWPE is used for HAp/polymer reinforcement. HAp nanorods prepared by 24 h hydrothermal reaction were mixed with HMWPE. Before mixing, HMWPE and HAp nanoparticles were dried in an oven at 120 °C for 1 h and cooled down to room temperature to remove the moisture contents. 10% of HAp nanorods prepared by hydrothermal reaction were mixed with the HMWPE. The blending was carried out in a high speed rotating kneader with the mixing temperature of 180 °C. A mixing time of 20 min was fixed for all the samples and the rotor speed at 80 rpm. A horizontal injection moulding machine was used for preparing specimen to study the mechanical behaviour. Before the tensile testing, the width and thickness of the specimens were measured with a micrometer. For comparison, pure HMWPE specimen and the HAp prepared by precipitation method also reinforced with HMWPE and tested for their mechanical strength.

Characterization

All the samples prepared by the hydrothermal reaction were structurally characterized by using X-ray diffraction pattern using Cu-$K\alpha_1$ radiation (RIGAKU X-RAY DIFFRACTOMETER D/MAX-2200). The morphology, particle size, and size distribution of particles were investigated by a field emission scanning electron microscope (FESEM JEOL JSM-6500) at 10 kV after sputtering the conducting platinum coating on the powder samples. To provide further insight into the nanostructures of the rods, analytical transmission electron microscopic (TEM) investigations were also performed using JEOL JEM-2100. Samples for electron microscopy were prepared by air-drying a drop of a sonicated suspension of the dried precipitate in ethanol onto copper grids. Selected area electron diffraction (SAED) pattern and HRTEM analysis were also performed to know the crystallinity and the lattice spacing of the sample. The specific surface area of the prepared nanorods was measured by nitrogen gas adsorption method using BET 201-APCW surface area analyzer. The Fourier transform infrared spectrum was obtained by using the KBr technique. The sample was blended with KBr in a 1:1 M ratio and pressed into a disk. The measurements were done in the range from 400 to 4000 cm^{-1} at an interval of 4 cm^{-1} averaging 20 scans. The FTIR analysis was performed by using a SHIMADZU FTIR 8000S. The tensile experiment was performed with a universal testing machine (810 Material Test Systems) at a crosshead speed of 50 mm/min. Young's modulus was calculated from the initial linear region of the stress–strain curves. The yield strength was determined from the upper yield point and the fracture strain was the elongation at break from the tensile curve. The reported mechanical properties were calculated by averaging measurements of five specimens. The abrasion resistance of the specimens was evaluated by means of a Taber type abrasion tester. Weight loss during 30,000 rotations on a surface was measured to determine the abrasion resistance.

Finally, the thermogravimetric and differential thermal analysis (TG/DTA) were carried out using SDT Q600 V20 at the heating rate of 10 °C/min from room temperature to 800 °C in nitrogen atmosphere.

Results and discussion

X-ray diffraction analysis (XRD)

Figure 1a–d shows the XRD pattern of HAp nano particles synthesized by 6, 12, 18 and 24 h hydrothermal reaction and calcined at 600 °C for 2 h. For all reaction times, the XRD peaks were well defined, and it indicates that the samples were well crystallized. There are clear reflections from the HAp planes (002) at about 25.75° and (211), (112), (300), and (202) in the range 31°–35°. All the diffraction peaks could be readily indexed to the pure hexagonal phase [space group: $P6_3/m$ (176)] with the lattice parameters of $a = 9.418$ Å and $c = 6.884$ Å, which was in accordance with that of bulk HAp crystals. (JCPDS card # 09-0432).

Figure 1 clearly shows that the samples treated at 6 and 12 h has less peak intensity when compared to that of 18 and 24 h, which indicates that the samples reacted for a longer time in the hydrothermal reaction has a higher crystallinity when compared to that of shorter reaction time. In addition, it was found that the peak corresponding to (002) plane is the only peak that gains a substantial increase in relative intensity and the relative increase in the intensities of the other peaks are less and it indicates that the nanorods growth may occur along the (001) direction, that is, the *c*-axis direction as the reaction time is increased. Notably, increase in the hydrothermal reaction time improved the crystallinity being on the order 24 > 18 > 12 > 6 h. The average crystallite size was calculated from Scherrer's formula. The (002) peak was chosen to calculate the average crystallite size since the peak was developed well and separate from others; also the apatite crystal is known to grow along the *c*-axis direction preferentially. A similar trend was also observed in the crystal size as observed in the crystallinity. There is an increase in the crystallite size with increasing hydrothermal reaction time. The crystallite sizes calculated are plotted in the Fig. 2 and there is a small increase in crystallite size from 17 to 21 nm when we increase the reaction time.

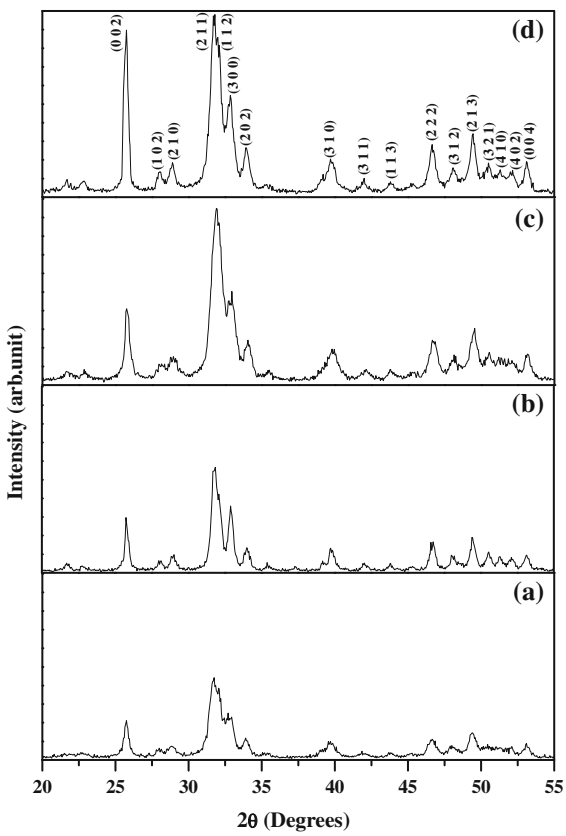

Fig. 1 XRD pattern of the HAp sample prepared by hydrothermal reaction for (*a*) 6 h, (*b*) 12 h, (*c*) 18 h (*d*) 24 h and calcined at 600 °C for 2 h

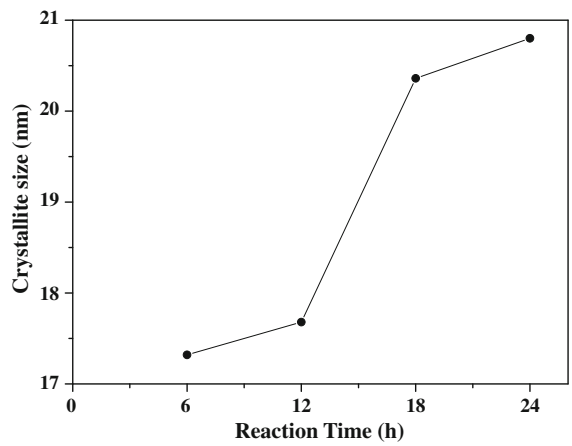

Fig. 2 Crystallite size of the HAp sample prepared by hydrothermal reaction for different time and calcined at 600 °C for 2 h

The lattice parameters were calculated for all the four samples hydrothermally treated from 6 to 24 h. Both values, ~9.41–9.42 Å for the *a*-axis and ~6.88–6.89 Å for the *c*-axis, showed that there are no significant changes with the hydrothermal reaction time and these were very close to the reported value for pure bulk HAp [$a = 9.418$ Å and $c = 6.884$ Å]. It is particularly noteworthy that the lattice parameters (both *a*- and *c*-axis in all apatite) varied a little with heat treatment. But in our case, the reaction time does not affect the lattice parameter notably.

Field emission scanning electron microscopic analysis (FESEM)

The morphology of the hydrothermally synthesized powders, observed by FESEM, is shown in Fig. 3. Figure 3a shows the typical FESEM image of the HAp nano particles synthesized by 6 h hydrothermal reaction. The morphology shows the particles with sphere-like structure exhibiting a non-uniform size distribution. Also, particles with small rod shape have been barely observed which revealed that the nucleation of the initial nanoparticles are started to form the nanorods after 6 h hydrothermal reaction. FESEM image of the 12 h hydrothermally reacted HAp particles (Fig. 3b) reveals the formation of nanorods with lengths in the range from 80 to 100 nm and width around 20 to 40 nm. After 12 h reaction, we could also observe both types of morphologies, but the concentration of the rod-like morphology is increased compared to sphere-like morphology, and it is shown in Fig. 3b. These observations clearly indicate that the growth of the nanorods is at the cost of small particles and also depends on the reaction time in the hydrothermal process. Prolonged reaction time of 18 h (Fig. 3c) showed the formation of large number of nanorods with almost well-defined morphology with typical widths of 30 to 50 nm and lengths in the range from 100 to 130 nm. It should be noted that the sphere-like structures had almost disappeared in the FESEM for this 18 h reacted sample which indicate the fact that the nucleation of the small particles increases as the reaction time increases and form the rod like morphology. Again, 24 h hydrothermally reacted samples (Fig. 3d) have shown the formation of ripened and well defined shape nanorods with a diameter of ~15 nm and with length of ~150 nm. This nanostructure shows that this particular sample has almost uniform distribution of size and shape of the nanorods. It is noted that each sample has uniform rod-like particles with slightly different aspect ratios which is around 8–10 (i.e. length/diameter). Thus, the surface morphological analysis of the obtained nanoparticles has clearly revealed the piece of information about the nucleation and the growth of the nanorods. Also, the morphology of the hydrothermally treated HAp at different reaction times shows that the growth of the nanorods well depends on the reaction time. The morphology of the HAp particles prepared by precipitation method which is used for the comparison of the mechanical strength analysis was also shown in Fig. 3f. The morphology shows the irregular shape of the particle and the particle size is of the order of 5–20 μm.

Transmission electron microscopic analysis (TEM)

TEM and HRTEM images provide (Fig. 4) a further insight into the nanostructure and morphology of the prepared HAp, and the observed results were in good agreement with SEM and XRD results. Thus, from the TEM and XRD analysis, they reveal that the material has the compact crystal structure of apatite. Figure 4a shows the bright-field TEM image of the 6 h hydrothermally reacted sample. It shows that the sample contains small spherical particles with the size range of ~20–25 nm. The inset shows the corresponding SAED pattern of the same sample which shows the polycrystalline nature. Figure 4b and c shows TEM images of the HAp samples prepared by 12 and 18 h hydrothermal reaction. The morphology clearly shows the development of the rod like structure. Figure 3d shows the HAp particles prepared by 24 h hydrothermal reaction. It clearly reveals the formation of very fine nanorods with a diameter of ~15 nm and length in the range of ~100 to 130 nm. The corresponding SAED and HRTEM images are shown in Fig. 4e. The SAED patterns on different positions of a given single nanorod were essentially identical, thus indicating that the nanorods are single-crystalline. The discrete SAED spots demonstrate that the prepared HAp is well-crystallized hexagonal single crystal. The HRTEM reveals that the growth of typical HAp crystal is along the (002) plane which also confirmed through the XRD studies. It is known that in human bone the HAp

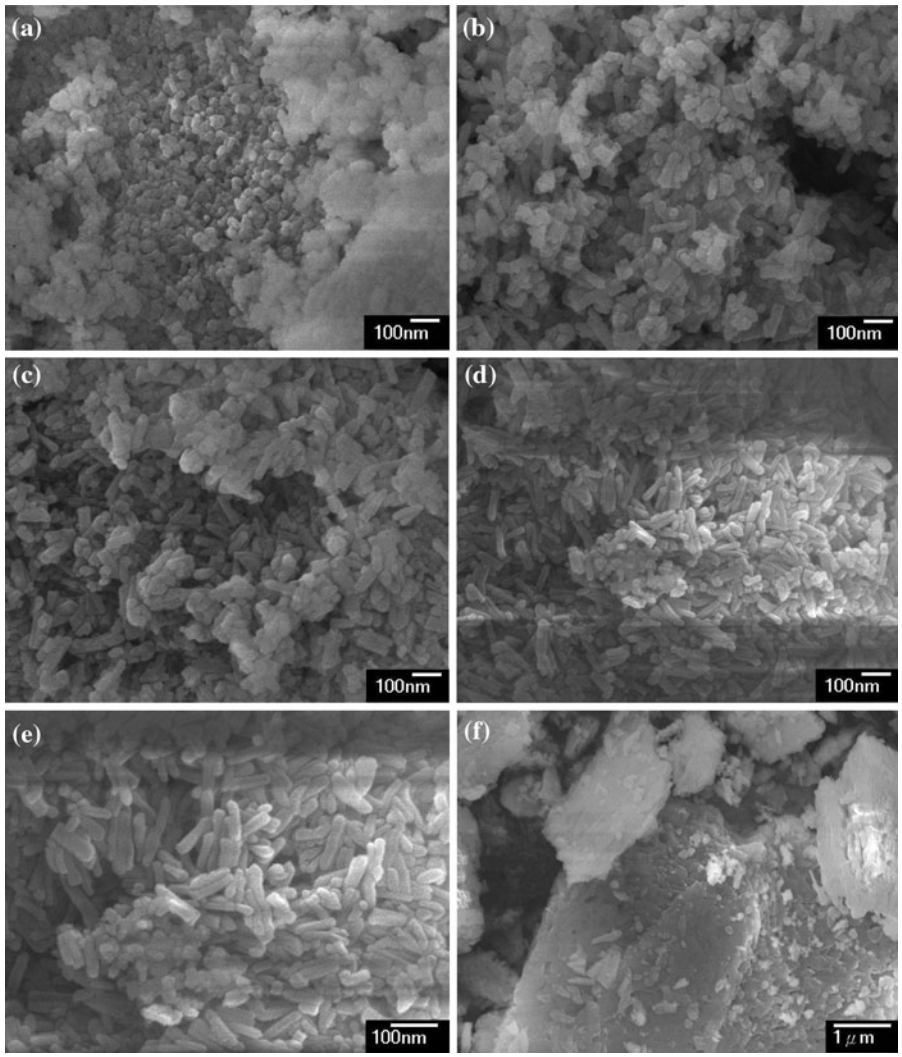

Fig. 3 FESEM of the HAp nanorods prepared by hydrothermal reaction for **a** 6 h, **b** 12 h, **c** 18 h, **d** 24 h and calcined at 600 °C. **e** Magnified image of **d**, and **f** morphology of the HAp particles prepared by precipitation method

crystals grow in parallel with the collagenous fiber along the (002) *c*-axis (Chang et al. 2003). More detailed TEM and SEM analyses of the HAp nanorods give an average diameter of about ~15 nm and the length ranging from 130 to 150 nm. The aspect ratio of the nanorods is increased from 2 to 10 as the hydrothermal reaction time is increased from 6 to 24 h.

The interplanar distances measured in segments (fringes) of the HRTEM micrograph of 24 h reacted sample were ~0.35 nm, corresponding to the interplanar spacing of the (002) plane of the hexagonal HAp. The preferred growth direction of the nanorods appears to be parallel to the (001) direction of the hexagonal HAp, indicating that the nanorod growth is along the *c*-axis direction of HAp.

For a complete view of the formation process of the HAp nanorods and their growth mechanism, a detailed time dependent morphology evaluation study was conducted at 180 °C hydrothermal reaction. Based on the above time-dependent morphology evaluation evidence, the formation process of the nanorods can be proposed as follows: the conventional hydrothermal crystallization process is a transformation process in which amorphous fine nanoparticles act as the precursor. The formation of tiny crystalline nuclei occurred first and then followed by nucleation upon increasing

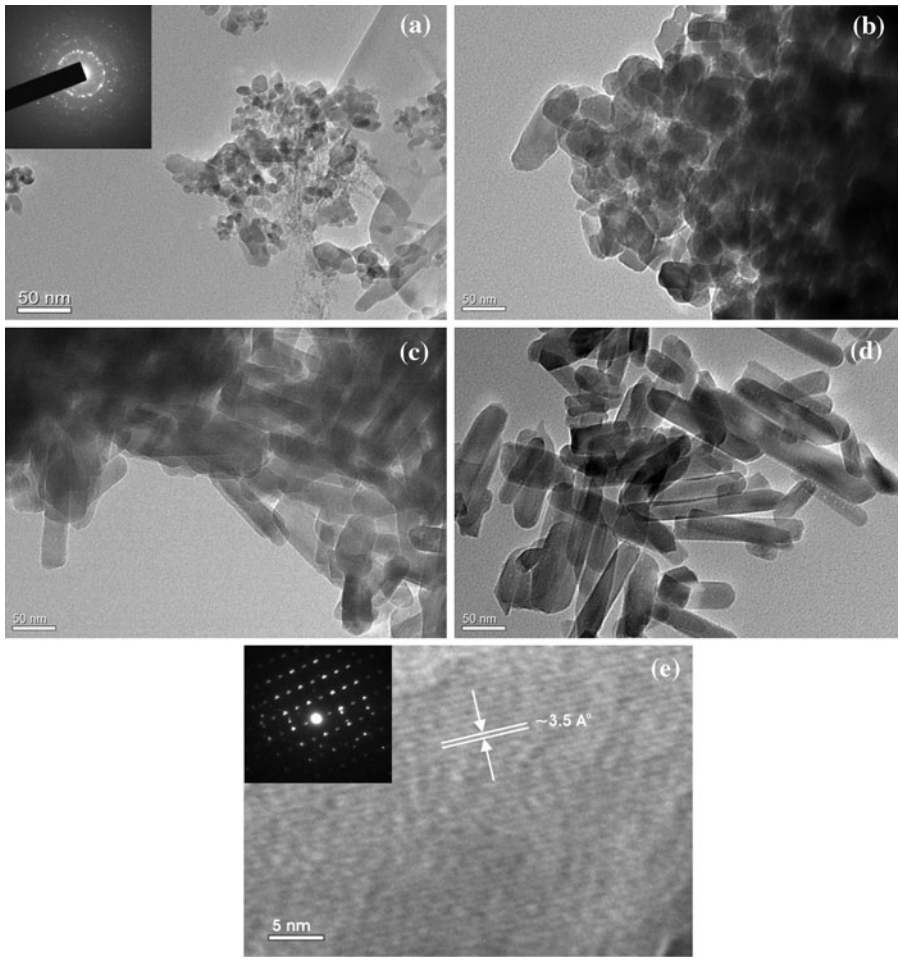

Fig. 4 TEM of the HAp nanorods prepared by hydrothermal reaction for **a** 6 h (*inset*: SAED pattern of sample), **b** 12 h, **c** 18 h, **d** 24 h and **e** HRTEM image of (sample **d**). *Inset*: SAED pattern of single nanorod from sample (**d**)

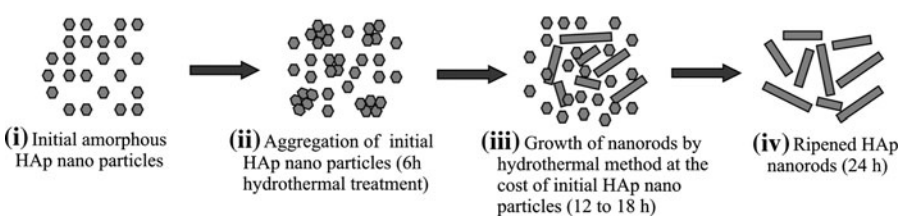

Fig. 5 Schematic representation of the HAp nanorods formation by hydrothermal method

the reaction time. The large particles will grow at the expense of the small ones due to a higher solubility of the small particles than that of large particles. In the early stage of nucleation, the examination of intermediate products shows the coexistence of the short rods and irregular nanoparticles which vanished and leading to the formation of longer nanorods. The formation process of nanorods can be schematically illustrated in Fig. 5. We also studied the morphology of the HAp prepared by 36 h hydrothermal reaction time. But there is no significant change when compared to that of 24-h reaction time.

BET specific surface area analysis

The specific surface area (defined as the surface area divided by the mass of the relevant phase) of the nanorods prepared by 24 h hydrothermal reaction shows 66.74 m^2/g found out by nitrogen adsorption method. For comparison, the specific surface area of

the HAp prepared by the precipitation method also analyzed, and the value is 14.71 m^2/g. There is a huge difference between hydrothermally reacted HAp nanorods and the precipitated HAp particles. The nanorods prepared by the hydrothermal method have a higher surface area with low mass because of the defined structure and the size. But in the case of the precipitated particles, it has not possessed any specific shape and size. So the specific surface area may be very low in the case of the precipitated HAp particles. This confirms the advantage of the hydrothermally reacted HAp nanorods over the precipitated particles.

Fourier transform infra red analysis (FTIR)

The hydrothermally synthesized samples were characterized by using the FTIR spectroscopic analysis and the spectrum of the 24 h hydrothermally reacted sample is shown in Fig. 6. The characteristic bands for PO_4^{3-}appear at 472, 583, 601, 961, 1032, and 1108 cm^{-1} (Blakeslee and Condrate 1971). The trace at 472 cm^{-1} is attributed to the $v2$ bending vibration. The triply degenerated $v4$ bending vibrations are reflected as traces at 583 and 601 cm^{-1}. The band at 961 cm^{-1} corresponds to $v1$ and the bands at 1032 and 1108 cm^{-1} to the $v3$ vibrations of PO_4^{3-} ions (Markovíc et al. 2004). It is generally expected that the absorption of the CO_3^{2-} peaks would be pronounced if the Ca/P ratio is greater than the stoichiometric value (Aizawa et al. 2006). But, as the HAp was synthesized from a strictly stoichiometric Ca/P precursor mixture (Ca/P = 1.67), we could not observe any peak corresponding to CO_3^{2-}. But the carbonate ions are a common impurity in HAp (Cho et al. 2005). The broad and high-intensity band extending from 2500 to 3600 cm^{-1} derives from the $v3$ and a $v1$ stretching mode of the hydrogen-bonded H_2O molecules and the band at 1642 cm^{-1} derives from the $v2$ bending mode of the H_2O molecules. The bands at 3573 and 632 cm^{-1} arise from the stretching and vibrational modes, respectively, of the OH^- ions (Chen and Liang 2007; Cheng et al. 1998).

Mechanical studies

Exemplary stress–strain curves for the median specimen in each experimental group qualitatively depict the overall effects of the reinforcement type on the composite mechanical properties in tension (Fig. 7) and abrasion (Fig. 8). The tensile properties were measured from the tensile curves, and it is summarized in Table 1. From the stress–strain curve, there is an initial increase followed by a decrease in the ultimate tensile stress for all the three samples. A maximum ultimate tensile stress of approximately 38.64, 39.05 and 43.02 MPa for pure HMWPE, HMWPE with 10% HAp NR and HMWPE with 10% HAp particle, respectively, was achieved. It is also expected that the reinforcement resulted in a decrease in the elongation at break (work to failure) for either type of reinforcement. HAp nanorod reinforcement had higher elastic modulus, ultimate tensile strength and work to failure relative to

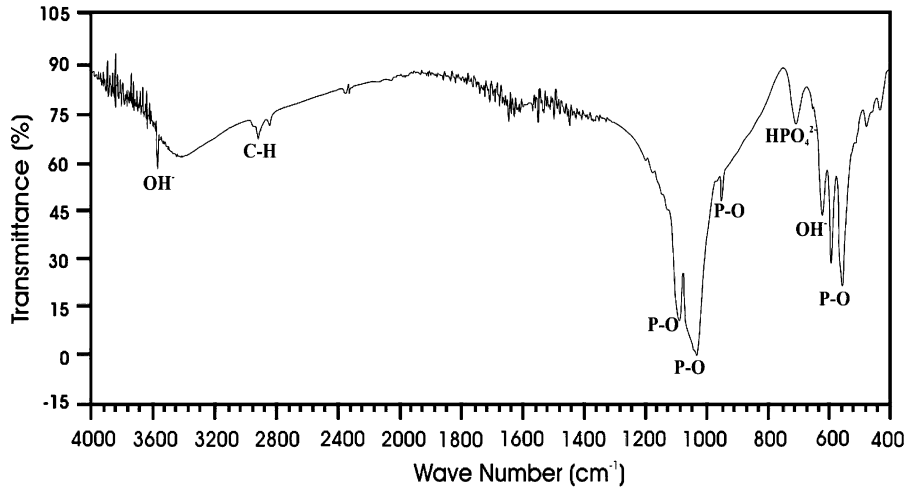

Fig. 6 FTIR spectra for the 24 h hydrothermally reacted HAp nanorods calcined at 600 °C

composite reinforced with precipitated HAp. As expected, the reinforcement resulted in increased elastic modulus, a maximum in ultimate tensile stress and decreased work to failure. There is only a slight decrease in the elongation at break (work to failure) for HAp nanorods compared to pure HMWPE. The large change in the work to failure with reinforcement of HAp particles prepared by the precipitation method and the changes in the shape of stress–strain curves in Fig. 7 suggest that a transition from ductile to brittle failure occurred in a little while than that of other two specimens. Thus, HAp nanorod reinforced HMWPE composites possessed enhanced mechanical properties over that reinforced with precipitated HAp particles. The strengthening effects observed for HAp nanorods over the precipitated HAp particles were thus concluded to be solely due to the morphology and the preferred orientation of the reinforcement phase (Roeder et al. 2003).

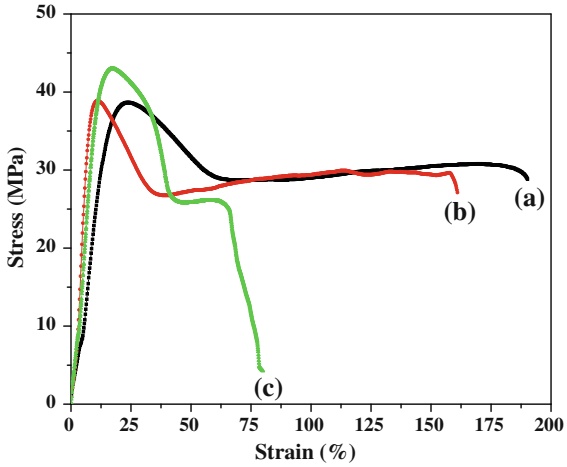

Fig. 7 Typical stress–strain curve of **a** pure HMWPE, **b** HMWPE/HAp NRs, and **c** HMWPE/HAp particle reinforcement

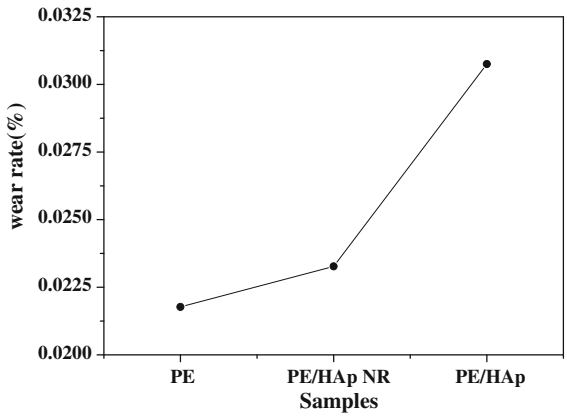

Fig. 8 Wear rate of the HMWPE and HMWPE/HAp reinforcement

Abrasion resistance of the HAp particles reinforced with HMWPE are shown in the Fig. 8. It is found that the abrasion resistance increases with decrease in particle size and the well defined shape.

Compared to precipitated HAp, the increase in the mechanical strength may be the result of the combined effects of (1) increased grain-boundary sliding mechanism due to large number of grain boundaries present in nanophase ceramics and (2) smaller diameter of individual surface pores present on nanophase ceramics (Webster et al. 1999; Siegel and Fougere 1995; Webster 2001). For these reasons, the HAp nanorods provide a preferable alternative to conventional orthopedic and dental implants that fail due to crack initiation and propagation during in vivo loading. The results in this article provide further evidence that nanophase ceramics may be synthesized to match mechanical properties of bone and thus demonstrated strong promise and potency for their use in orthopedic and dental implant applications.

It is reported that the mechanical properties of bioceramics similar to human bone can be obtained by decreasing the grain size of ceramic formulations into the nanometer regime. Such mechanical properties must be incorporated into bioceramics for orthopedic and dental applications; mechanical properties similar to those of physiological bone are needed in order to

Table 1 Mechanical properties of HMWPE and HAp/HMWPE composites

Sample	Young's modulus (GPa)	Yield strength (MPa)	Elongation at break (%)	Wear rate (%)
HMWPE	0.85	38.64	190.2	0.02177
HMWPE + 10 wt% HAp NR	3.92	39.05	160.8	0.02327
HMWPE + 10 wt% HAp	3.79	43.02	79.69	0.03075

minimize imbalances in stress and strain distributions at the tissue implant interface, which often lead to bone resorption and eventual implant loosening and failure (Webster 2001).

Extended strain to failure has been well documented for submicrometer and nanocrystalline ceramics; in this study, elongation to failure of 160.8% was achieved for the HAp nanorods reinforced polyethylene, whereas the elongation to break is only 79.69% for precipitated HAp particles. From the SEM images, we can clearly observe the sizes of the HAp nanorods as well as precipitated HAp particles. As reported earlier, the extended strain to failure for the HAp nanorods is mainly due to the decreasing size of the particles in the nanometer range.

Along with the particle size and shape, the homogeneous mixing with the polymer matrix is also affecting the mechanical strength. In the precipitation method, the particles are aggregated with each other and also the particle size is very high when compared to that of the hydrothermal method. Due to the aggregation and the bigger particle size, the homogeneous mixing with HMWPE was very difficult compared to that of HAp nanorods which will affect the mechanical strength. But in the case of the HAp nanorods, the size and the shape of the nanorod is well defined, and the smaller size provide a well homogenous mixture of HAp and HMWPE which shows the good mechanical strength. In conclusion, the HAp nanorods prepared by hydrothermal reaction shows the better mechanical strength when compared to the HAp prepared by precipitation method.

Thermogravimetric analysis (TG–DTA)

The TG–DTA curve for the as-prepared HAp, obtained by heating up to 800 °C in nitrogen atmosphere is shown in Fig. 9. Regardless of the reaction time (6–24 h), the curves behaved in a similar manner. From the TG analysis, the initial gradual weight loss of 5% at $T_{room} \leq T \leq 218$ °C and this may be due to the loss of adsorbed or hydration water molecules. The next weight loss is of 21% at 218 °C $\leq T \leq$ 310 °C. This second weight loss corresponds to the nitrate decomposition. Over the temperature interval, 310 °C $\leq T \leq$ 600 °C, there is a very slight slope attributed due to the release of gas inside the sample. From the DTA, exothermic processes registered at 250 °C $\leq T \leq$ 500 °C show the crystallization of HAp. The strong peak at 287 °C (exothermic) corresponds to the nitrate decomposition.

For the HMWPE reinforcement, it can be found that overall crystallization of HMWPE becomes faster by the addition of HAp crystals. From DTA curves (Fig. 10), it can be seen that, filler loading has not much influence on the crystallisation of HMWPE. Melting temperature of pure HMWPE is around

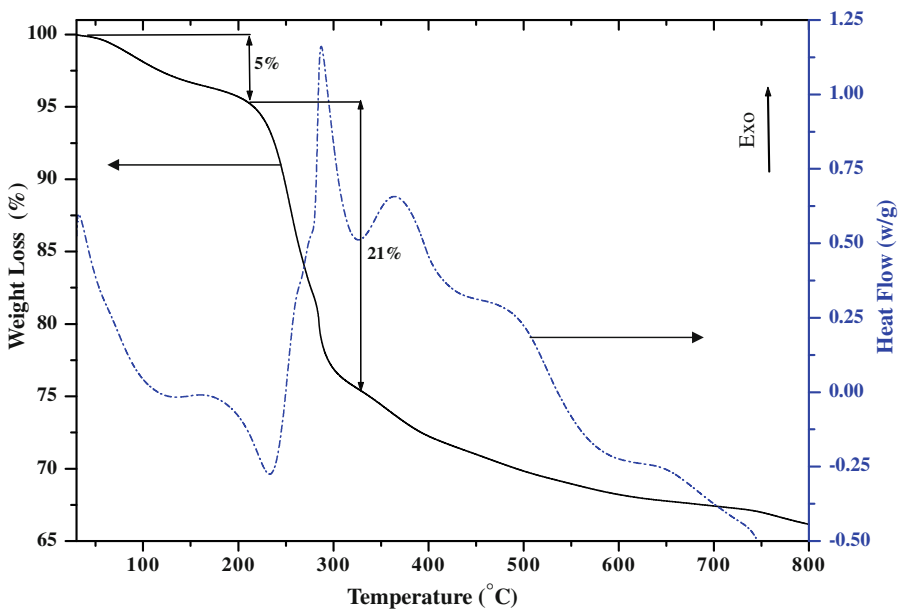

Fig. 9 TG-DTA curve for the as prepared 24 h hydrothermally reacted HAp nanorods

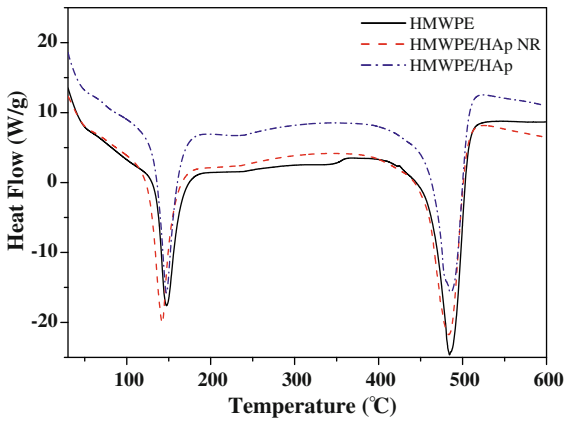

Fig. 10 DTA curve for the HMWPE, HMWPE/HAp NR, HMWPE/HAp

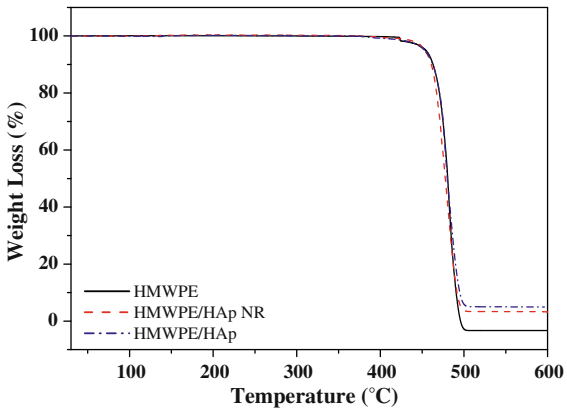

Fig. 11 TG curve for the HMWPE, HMWPE/HAp NR, HMWPE/HAp

150 °C as expected for the commercial samples. Increase in melting temperature upon filler loading is negligible. Generally addition of HAp does not change crystallinity of HMWPE. TGA curves of HMWPE and its composites (Fig. 11) show only one-step degradation for pure HMWPE and its composites.

Conclusion

The purpose of this study was to elucidate the experimental results of the synthesis and the mechanical properties of the well defined and single crystalline HAp NRs reinforced with HMWPE. HAp nanoparticles with uniform morphologies and controllable size have been synthesized by simple hydrothermal reaction by varying the reaction time without using surfactant and/or templating agents and the morphology of the HAp is vary such as spheres, nanorods, and increase in the length of nanorod by varying the reaction time. The prepared HAp nanorods had a length of about 100–150 nm and the diameter of about 15–20 nm. SAED and HRTEM analysis revealed the single crystalline nature of the nanorods and having the preferred growth along (001) direction. The measured interplanar distances in HRTEM micrograph shows ~0.35 nm, which corresponds to the interplanar spacing of the (002) plane of the hexagonal HAp. This confirms the nanorod growth is along the *c*-axis direction of HAp. The improvement in the tensile properties and abrasion resistance were observed for the HAp nanorods reinforced with HMWPE compared with HAp precipitates reinforced with HMWPE. The strengthening effects observed for HAp nanorods over the precipitated HAp particles were thus concluded to be solely due to the morphology and the preferred orientation of the reinforcement phase.

Acknowledgments One of the authors AJN gratefully acknowledges the financial support from the Ministry of Higher Education, Taiwan, through Taiwan-India Collaborative Research Project. The authors also thank Mr. Wu Jun Jie and Mr. Dann Yu for their help in taking FESEM and TEM analysis. We are also indebted to Centre for EMO Materials and Nanotechnology, National Taipei University and Technology for Mechanical studies.

References

Aizawa M, Ueno H, Itatani K, Okada I (2006) Syntheses of calcium-deficient apatite fibers by a homogeneous precipitation method and their characterizations. J Eur Ceram Soc 26:501–507

Anmin H, Tong L, Ming L, Chengkang C, Huiqin L, Dali M (2006) Preparation of nanocrystals hydroxyapatite/TiO_2 compound by hydrothermal treatment. Appl Catal B 63:41–44

Blakeslee KC, Condrate RA (1971) Vibrational spectra of hydrothermally prepared hydroxyapatites. J Am Ceram Soc 54:559–563

Cao M, Wang Y, Guo C, Qi Y, Hu C (2004) Preparation of ultrahigh-aspect-ratio hydroxyapatite nanofibers in reverse micelles under hydrothermal conditions. Langmuir 20: 4784–4786

Chang MC, Ko C, Douglas WH (2003) Preparation of hydroxyapatite-gelatin nano composite. Biomaterials 24:2853–2862

Chen B, Liang C (2007) Preparation of hydroxyapatite coating by the use of a sacrificial Mg anode method. Ceram Int 33:701–703

Chen JD, Wang YJ, Wei K, Zhang SH, Shi XT (2007) Self-organization of hydroxyapatite nanorods through oriented attachment. Biomaterials 28:2275–2280

Cheng ZH, Yasukawa A, Kandori K, Ishikawa T (1998) FTIR study on incorporation of CO_2 into calcium hydroxyapatite. J Chem Soc Faraday Trans 94:1501–1505

Cho SH, Joo SM, Cho JS, Lee JK, Kim H (2005) Mechanical properties and workability of self-hardening calcium phosphate cement as a function of the particle size distribution. J Ceram Process Res 6:57–62

Di NS, Brovarone CV, Spriano S, Milanese D, Verne E, Bergo V, Maina G, Spinelli P (2004) Silver containing bioactive glasses prepared by molten salt ion-exchange. J Eur Ceram Soc 24:2935–2942

Elliott JC (1994) Structure and chemistry of the apatites and other calcium orthophosphates. Elsevier, Amsterdam

Elliott JC (1998) Recent studies of apatites and other calcium orthophospates. In: Bres E, Hardouin P (eds) Calcium phosphate materials, fundamentals. Sauramps Medical, Monpellier, p 25

Feng X, Ye J, Wang Y, Rao P (2005) Deagglomeration of HA during the precipitation synthesis. J Mater Sci 40(20): 5439–5442

Hench LL (1991) Bioceramics: from concept to clinic. J Am Ceram Soc 74:1487–1510

Hirai T, Hodono M, Komasawa I (2000) The preparation of spherical calcium phosphate fine particles using an emulsion liquid membrane system. Langmuir 16:955–960

Huang J, Lin YW, Fu XW, Best SM, Brooks RA, Rushton N et al (2007) Development of nano-sized hydroxyapatite reinforced composites for tissue engineering scaffolds. J Mater Sci Mater Med 18(11):2151–2157

Hulber SF, Bokros JC, Hench LL, Wilson J, Heimke G (1987) Ceramics in clinical applications: past, present and future. In: Vincenzini P (ed) High tech ceramics. Elsevier, Amsterdam, pp 189–213

Kobayashi S, Kawai W (2007) Development of carbon nanofiber reinforced hydroxyapatite with enhanced mechanical properties. Compos A 38:114–123

Lewandrowski KU, Bondre SP, Wise DL, Trantolo DJ (2003) Enhanced bioactivity of a poly(propylene fumarate) bone graft substitute by augmentation with nano-hydroxyapatite. Biomed Mater Eng 13(2):115–124

Lin K, Chang J, Cheng R, Ruan M (2007) Hydrothermal microemulsion synthesis of stoichiometric single crystal hydroxyapatite nanorods with mono-dispersion and narrow-size distribution. Mater Lett 61:1683–1687

Maquet V, Boccaccini AR, Pravata L, Notingher I, Jerome R (2004) Porous poly(α-hydroxyacid)/Bioglass^R composite scaffolds for bone tissue engineering. I: preparation and in vitro characterisation. Biomaterials 25:4185–4194

Markovíc M, Flower BO, Tung MS (2004) Preparation and comprehensive characterization of a calcium hydroxyapatite reference material. J Res Natl Inst Stand Technol 109:553–568

Mathieu LM, Mueller TL, Bourban PE, Pioletti DP, Muller R, Manson JAE (2006) Architecture and properties of anisotropic polymer composite scaffolds for bone tissue engineering. Biomaterials 27:905–916

Ramay HRR, Zhang M (2004) Biphasic calcium phosphate nanocomposite porous scaffolds for load-bearing bone tissue engineering. Biomaterials 25:5171–5180

Rodriguez-Lorenzo LM, Vallet-Regi M (2000) Controlled crystallization of calcium phosphate apatites. Chem Mater 12:2460–2465

Roeder RK, Sproul MM, Turner CH (2003) Hydroxyapatite whiskers provide improved mechanical properties in reinforced polymer composites. J Biomed Mater Res 67A:801–812

Sarda S, Heughebaert M, Lebugle A (1999) Influence of the type of surfactant on the formation of calcium phosphate in organized molecular systems. Chem Mater 11:2722–2727

Shen Z, Adolfsson E, Nygren M, Gao L, Kawaoka H, Niihara K (2001) Dense hydroxyapatite-zirconia ceramic composites with high strength for biological applications. Adv Mater 13:214–216

Shi Z, Huang X, Cai Y, Tang R, Yang D (2009) Size effect of hydroxyapatite nanoparticles on proliferation and apoptosis of osteoblast-like cells. Acta Biomater 5:338–345

Shiha WJ, Wangb MC, Hona MH (2005) Morphology and crystallinity of the nanosized hydroxyapatite synthesized by hydrolysis using cetyltrimethylammonium bromide (CTAB) as a surfactant. J Cryst Growth 275:e2339–e2344

Siegel RW, Fougere GE (1995) Mechanical properties of nanophase metals. Nanostruct Mater 6:205–216

Suchanek W, Yashima M, Kakihana M, Yoshimura M (1997) Hydroxyapatite/hydroxyapatite-whisker composites without sintering additives: mechanical properties and microstructural evolution. J Am Ceram Soc 80:2805–2813

Sun Y, Guo G, Wang Z, Guo H (2006) Synthesis of single-crystal HAP nanorods. Ceram Int 32:951–954

Sun Y, Guo G, Tao D, Wang Z (2007) Reverse microemulsion-directed synthesis of hydroxyapatite nanoparticles under hydrothermal conditions. J Phys Chem Solids 68:373–377

Walsh D, Mann S (1996) Chemical synthesis of microskeletal calcium phosphate in bicontinuous microemulsions. Chem Mater 8:1944–1953

Wang M (2003) Developing bioactive composite material for tissue replacement. Biomaterials 24:2133–2151

Wang YJ, Zhang SH, Wei K, Zhao N, Chen JD, Wang XD (2006a) Hydrothermal synthesis of hydroxyapatite nanopowders using cationic surfactant as a template. Mater Lett 60:1484–1487

Wang YJ, Chen JD, Wei K, Zhang SH, Wang XD (2006b) Surfactant-assisted synthesis of hydroxyapatite particles. Mater Lett 60:3227–3231

Webster TJ (2001) Nanophase ceramics: the future orthopedic and dental implant material. In: Ying JY (ed) Nanostructured materials. Academic Press, San Diego, pp 125–160

Webster TJ, Siegel RW, Bizios R (1999) Design and evaluation of nanophase alumina for orthopaedic/dental applications. Nanostruct Mater 12:983–986

Wei G, Ma PE (2004) Structure and properties of nano-hydroxyapatite/polymer composite scaffolds for bone tissue engineering. Biomaterials 25:4749–4757

Yang W, Araki H, Kohyama A, Thaveethavorn S, Suzuki H, Noda T (2004) Fabrication in situ SiC nanowires/SiC

matrix composite by chemical vapour infiltration process. Mater Lett 58:3145–3148

Yaszemski MJ, Payne RG, Hayes WC, Lander R, Mikos AG (1996) Evolution of bone transplantation: molecular, cellular and tissue strategies to engineer human bone. Biomaterials 17:175–185

Yuan ZY, Liu JQ, Peng LM (2002) Morphosynthesis of vesicular mesostructured calcium phosphate under electron irradiation. Langmuir 18:2450–2452

Zhang F, Zhou ZH, Yang SP, Mao LH, Chen HM, Yu XB (2005) Hydrothermal synthesis of hydroxyapatite nanorods in the presence of anionic starburst dendrimer. Mater Lett 59:1422–1425

Zhu K, Yanagisawa K, Onda A, Kajiyoshi K (2004) Hydrothermal synthesis and morphology variation of cadmium hydroxyapatite. J Solid State Chem 177:4379–4385